RESEARCH ARTICLE
doi: 10.2306/scienceasia1513-1874.2024.076

ScienceAsia 50 (4): 2024: ID 2024076: **1–9**

11β- hydroxysteroid dehydrogenase type 1 selective inhibitor alleviates insulin resistance and non-alcoholic fatty liver disease in db/db mice

Wen-wen Qi[a], Yong Liu[b], Peng-fei Liu[c], Mei Yi[b], Chao Zhang[b], Shuang Zhang[d], Li-Yong Zhong[a,*]

[a] Department of Endocrinology, Beijing Tiantan Hospital, Capital Medical University, Beijing 100070 China
[b] Department of Ultrasound, Beijing Shijitan Hospital, Capital Medical University, Beijing 100038 China
[c] Department of Anesthesiology, Beijing Shijitan Hospital, Capital Medical University, Beijing 100038 China
[d] Department of Pathology, Beijing Shijitan Hospital, Capital Medical University, Beijing 100038 China

*Corresponding author, e-mail: zhongliyong@bjtth.org

Received 27 May 2023, Accepted 6 Jul 2024
Available online 19 Sep 2024

ABSTRACT: Non-alcoholic fatty liver disease, often linked to insulin resistance, is associated with increased expression of 11β-hydroxysteroid dehydrogenase type 1 (11β-HSD1) in liver tissue. We here assessed the effects of the 11β-HSD1 inhibitor BVT.2733 on non-alcoholic fatty liver disease and its underlying mechanisms. Mice were divided into three groups: control, db/db, and db/db +BVT.2733. After 4 weeks, serological testing was conducted, and glucose tolerance and insulin sensitivity were assessed. The severity of non-alcoholic fatty liver disease was evaluated using B-ultrasound, Hematoxylin and Eosin staining, and Oil Red O staining. Liver corticosterone levels were measured using enzyme-linked immunosorbent assay. Liver expression of 11β-HSD1, Phosphatidylinositol 3-kinase (PI3K) -Serine-Threonine kinase (AKT)-Mammalian target of rapamycin (mTOR) signaling pathway-related proteins, and autophagy-related proteins were analyzed by western blot. The results indicated that the leptin receptor-deficient mice db/db showed significant glucolipid metabolism disorder, insulin resistance, and increased non-alcoholic fatty liver disease severity, compared with the control group. BVT.2733 treatment ameliorated these conditions. Specifically, BVT.2733 downregulated liver 11β-HSD1 expression, resulting in reduced liver corticosterone levels. Additionally, BVT.2733 enhanced hepatocyte autophagy, activated the PI3K-AKT signaling pathway and inhibited the mTOR signaling pathway. These findings suggest that BVT.2733 not only improves glucolipid metabolism and insulin resistance but also mitigates non-alcoholic fatty liver disease, in leptin receptor-deficient mice db/db. The underlying mechanism likely involves decreased liver corticosterone levels and enhanced hepatocyte autophagy, mediated by the PI3K-AKT and mTOR signaling pathways.

KEYWORDS: 11β-HSD1, insulin resistance, NAFLD, PI3K-AKT-mTOR, autophagy

INTRODUCTION

Insulin resistance refers to the weakened biological response of the body to a certain concentration of insulin [1]. In severe cases, it can lead to non-alcoholic fatty liver disease (NAFLD), considered the hepatic manifestation of insulin resistance [2, 3]. Furthermore, NAFLD is associated with the high expression of 11β-hydroxysteroid dehydrogenase type 1 (11β-HSD1) in liver tissues [4].

11β-HSD1 is a glucocorticoid reductase that converts inactive cortisone into active cortisol. In rodents, it converts 11-dehydrocorticosterone to its active form, corticosterone (CORT), with high expression in liver, muscle, and adipose tissues [5]. 11β-HSD1 amplifies the biological effects of local glucocorticoids in tissues, disrupting glucose and lipid metabolism and exacerbating insulin resistance [4]. Moreover, knocking out the 11β-HSD1 gene or using an 11β-HSD1 inhibitor alleviates insulin resistance, by decreasing gluconeogenesis [6] and increasing glucose uptake by skeletal muscle [7]. However, the mechanism by which 11β-HSD1 alleviates NAFLD remains unclear.

The Phosphatidylinositol 3-kinase (PI3K)-Serine-threonine kinase (AKT) -Mammalian target of rapamycin (mTOR) signaling pathway is a classic insulin signaling pathway, involved in the synthesis of glycogen, lipids and proteins. Abnormalities in this pathway result in insulin resistance [8]. Glucocorticoids have a direct inhibitory effect on the PI3K-AKT pathway [9]. Meanwhile, mTOR is a significant regulator of autophagy initiation [10]. Autophagy is an intracellular degradation process that delivers cytoplasmic materials to the lysosome for degradation [11]. When autophagy is dysfunctional, the metabolism of adipose tissue, skeletal muscle, and liver is adversely affected [12]. Autophagy dysfunction also exacerbates hepatic steatosis in mice when inhibited by chloroquine [13]. Conversely, promoting autophagy relieve NAFLD [14].The use of autophagy enhancers like rapamycin or carbamazepine has a protective effect on high-fat diet-induced NAFLD by directly inducing hepatic autophagy [13]. Natural extracts such as resveratrol have also demonstrated the ability to improve NAFLD by enhancing autophagy [15]. Based on this, we hypothesize that, the 11β-HSD1 inhibitor alleviates insulin resistance and NAFLD, by reducing liver CORT levels, involving the PI3K-AKT-mTOR sig-

naling pathway, and promoting hepatocyte autophagy.

BVT.2733 has been identified as a novel 11β-HSD1 inhibitor. Leptin receptor-deficient mice db/db (db/db), serves as an animal model for spontaneous type 2 diabetes. These mice typically exhibit hyperglycemia, obesity, insulin resistance and NAFLD [16]. In this study, we assessed the effects of BVT.2733 on insulin resistance and NAFLD in db/db mice, focusing on its mechanism from the perspective of autophagy and the PI3K-AKT-mTOR signaling pathway.

MATERIALS AND METHODS

Animal grouping and model establishment

8-week-old male C57BLKSJ and db/db mice were maintained in the Animal Laboratory of Beijing Shijitan Hospital, Capital Medical University, in an environment with air circulation, a temperature of 22 °C–25 °C and a humidity of 40%–70%. The mice had free access to food and water. The experimental protocol was approved by the Animal Ethics Committee of Beijing Shijitan Hospital, adhering to the principles of animal welfare.

The mice were randomly assigned to three groups for a 4-week feeding experiment: control group (C57BLKSJ mice, $n = 9$), db/db group (db/db mice, $n = 9$), and db/db +BVT.2733 group (db/db mice treated with BVT.2733, $n = 9$). Each mouse in the db/db +BVT.2733 group received an intragastric administration of BVT.2733 (T2057, TargetMol Co. Ltd, USA) at a dose of 100 mg/kg/day. After 4 weeks, intraperitoneal glucose tolerance test (IPGTT), insulin tolerance test (ITT) and Type-B Ultrasonic test were performed. Subsequently, mice were anaesthetized with chloral hydrate, and blood samples and liver tissues were collected for further experiments.

IPGTT and ITT

To evaluate glucose tolerance and insulin sensitivity, IPGTT and ITT were conducted. For the IPGTT, glucose (2 g/kg) was injected intraperitoneally after overnight fasting. Blood samples were collected from the tail vein at 0, 15, 30, 60, 120 and 180 min after injection. For the ITT, insulin (1 U/kg) was injected intraperitoneally after a 4-h fasting. Blood samples were collected from the tail vein at 0, 30, 60, 90, and 120 min after injection. Blood glucose levels were measured by using a glucose meter (AccuCheck, Roche, Switzerland). The area under the curve generated from the data collected during the IPGTT or ITT was calculated using GraphPad Prism 9.0 (GraphPad, USA).

Type-B ultrasonic

To evaluate liver size and the degree of NAFLD, we examined the mice using Type-B Ultrasonic imaging. Since there is no precise method to calculate liver volume, we estimated the size by measuring the following diameters: the transverse diameter of the whole liver, the up-down diameter of the right liver lobe, the anterior-posterior diameter of the right liver lobe, and the anterior-posterior diameter of the left liver lobe. These measurements were taken using the LOGIQ E9 ultrasound imaging system. Due to the small size of the up-down diameter of the left liver lobe, it was not measured. The ML6-15 probe frequency was set at 15.0 MHz, under MSK SUP with a gain of 50 dB.

The degrees of NAFLD were classified into four grades: no fatty liver, mild fatty liver, moderate fatty liver, and severe fatty liver. The criteria are as follows: 1) No fatty liver: The normal liver has a homogeneous echogenic structure with an echogenic intensity equal to or slightly greater than that of the renal cortex and spleen. Due to fat infiltration, the liver's echogenic intensity surpasses that of the renal cortex and spleen. Various grades of steatosis have been proposed based on visual analysis of echo intensity. 2) Mild fatty liver: Slight increase in echogenicity with clear intrahepatic vascular boundaries and diaphragm. 3) Moderate fatty liver: Moderate increase in echogenicity, obscuring the echogenic walls of portal vein branches. 4) Severe fatty liver: Near-field diffuse punctate hyper-echogenicity with far-field echo attenuation, sparse light spots, and the echogenic liver obscuring the diaphragmatic outline. The intrahepatic duct structure is not clear. Three ultrasound doctors assisted with these examinations.

Serological detection

Fasting serum glucose, total cholesterol, triglyceride, alanine transaminase, and aspartate aminotransferase levels were measured using a Toshiba 120 automatic biochemical analyzer. The serum insulin levels were determined by radioimmunoassay, using ^{125}Iodine Insulin Radioimmunoassay Kit (S10930046, Beijing North Institute of Biotechnology Co., China), following the manufacturer's instructions. The homeostatic model assessment of insulin resistance (HOMA-IR) was calculated using the formula: HOMA-IR = serum glucose (mmol/l) × insulin (mU/l)/22.5.

Enzyme linked immunosorbent assay

Liver CORT levels were determined by enzyme linked immunosorbent assay, using the CORT Assay Kit (H205, Nanjing Jiancheng Bioengineering Institute, China), following the manufacturer's instructions. The results were analyzed with a Microplate Reader (Spark10M, Tecan, Switzerland) at 450 nm, ELISAcalc software was used for plotting the standard curve and data extrapolation.

Hematoxylin and eosin (HE) staining and NAFLD activity score

The liver tissues were washed with ice-cold phosphate buffer, fixed in 4% paraformaldehyde for 24 h, dehydrated through an alcohol gradient, cleared in xylene, and embedded in paraffin. The tissues were sliced into

5-µm sections using a microtome (KD-P, Zhejiang Kedi Instrumental Equipment Co., Ltd., Jinhua, China), conventionally dewaxed to water, and stained with HE to observe hepatocyte morphology.

The NAFLD activity score is the sum of three scores used for a semi-quantitative assessment of NAFLD progression. The steatosis score was based on the percentage of liver tissue affected: 0 (< 5%), 1 (5%–33%), 2 (> 33%–66%), and 3 (> 66%). The lobular inflammation score was determined by assessing inflammatory foci per field of view at a magnification of 200×: 0 (no foci), 1 (< 2 foci), 2 (2–4 foci), and 3 (> 4 foci). Hepatocyte ballooning was scored as follows: 0 (none), 1 (few ballooning cells), and 2 (many ballooning cells). Liver sections stained with HE were scored by a clinical pathologist.

Oil Red O (ORO) staining

ORO staining was used to detect fat droplets in the liver. After fixation in 4% paraformaldehyde for 24 h, liver tissues were immersed in 30% sucrose solution for 48 h at 4 °C for dehydration. The tissues were then embedded in an optimal cutting temperature compound (4583, Sakura, Japan) and sectioned into 8 µm slices using a cryotome (CM1860, Leica, USA). The sections were rinsed with 60% isopropanol for 2 min, stained with ORO working solution for 10 min, and then rinsed again with 60% isopropanol for 10 s. Finally, the sections were observed under a light microscope (Leica Biosystems, Shanghai, China). The ORO-positive area was calculated using ImageJ software (National Institutes of Health, USA).

Western blot

The isolated livers were homogenized in RIPA Lysis Buffer (P0013C, Beyotime , China) containing protease inhibitor (A8260, Solarbio, China) and protein phosphatase inhibitor (P1260, Solarbio), and then processed using an ultrasonic disruptor (UP-250, Tuohe Mechanical and Electrical Technology Co., Ltd., China). The lysates were centrifuged at 12000 rpm for 15 min at 4 °C, and the protein concentrations were measured using a bicinchoninic acid protein assay kit (P1513-2, Applygen, China). Equal volumes of proteins were separated by 4%–20% SDS/-PAGE gels (36231ES10, Yeasen, China) and transferred to PVDF membranes (Biosharp, China). The membranes were blocked in 5% skimmed milk for 2 h at room temperature and then incubated with primary antibodies against 11β-HSD1 (ab169785), and PI3K (ab191606), from Abcam, USA; phosphorylated PI3K (P-PI3K) (YP0224), AKT (YT0177), and phosphorylated AKT(p-AKT) (YT0006), from Immunoway, USA; mTOR (ab134903), phosphorylated mTOR(p-mTOR) (ab109268), microtubule-associated protein 1 light chain 3II/I (LC3II/I) (ab192890), and nucleoporin 62 (P62) (ab109012), from Abcam; β-actin (8H10D10, CST, USA); and β-tubulin (AF7011, Affinity Biosciences, USA) at 4 °C overnight. Subsequently, the membranes were incubated with secondary antibody goat anti-rabbit IgG (ab186694, Abcam) for 2 h at room temperature. The membranes were scanned using an infrared imaging system (Odyssey CLX, LI-COR, USA). Relative protein levels were calculated using ImageJ software (National Institutes of Health, USA), and the values were normalized to β-tubulin or β-actin.

Data analysis

Data were expressed as mean ± SD and analyzed using SPSS 26.0 (IBM, USA). The data distribution was evaluated using the Shapiro-Wilk test. For normally distributed data, differences between the three groups were analyzed by one-way analysis of variance followed by Bonferroni or Dunnett's multiple comparison test. For nonparametric data, differences were analyzed by the Kruskal-Wallis test followed by the Mann-Whitney U test. A repeated measures analysis of variance was used to compare group differences in the IPGTT or ITT. The degree of NAFLD was compared using Fisher's exact test. $p < 0.05$ was considered statistically significant.

RESULTS

BVT.2733 alleviates insulin resistance and glucolipid metabolism disorder in db/db mice

To assess the impact of BVT.2733 on insulin resistance and glucolipid metabolism disorder, db/db mice were utilized in this study. The experimental timeline is depicted in Fig. 1A. Compared with the db/db group, treatment with BVT.2733 significantly reduced the levels of fasting serum glucose, total cholesterol, triglyceride, serum insulin, and HOMA-IR ($p < 0.05$ or $p < 0.01$) (Fig. 1B–F). In IPGTT, mice treated with BVT.2733 exhibited faster glucose recovery ($p < 0.01$) (Fig. 1G). Similarly, in ITT, the glucose levels of the db/db +BVT.2733 group were lower than those of the db/db group ($p < 0.01$) (Fig. 1I). The area under the curve of IPGTT (Fig. 1H) and ITT (Fig. 1J) were significantly decreased in the db/db +BVT.2733 group, compared with the db/db group ($p < 0.05$ or $p < 0.01$). These findings indicate that BVT.2733 alleviates insulin resistance and glucolipid metabolism disorder in db/db mice.

BVT.2733 alleviates NAFLD in db/db mice

The efficacy of BVT.2733 in alleviating NAFLD was assessed in db/db mice. Treatment with BVT.2733 resulted in decreased serum alanine transaminase levels ($p < 0.01$) (Fig. 2A) and aspartate aminotransferase levels ($p < 0.05$) (Fig. 2B), compared with the db/db group. Compared with the control group, the db/db group exhibited increased transverse diameter of the

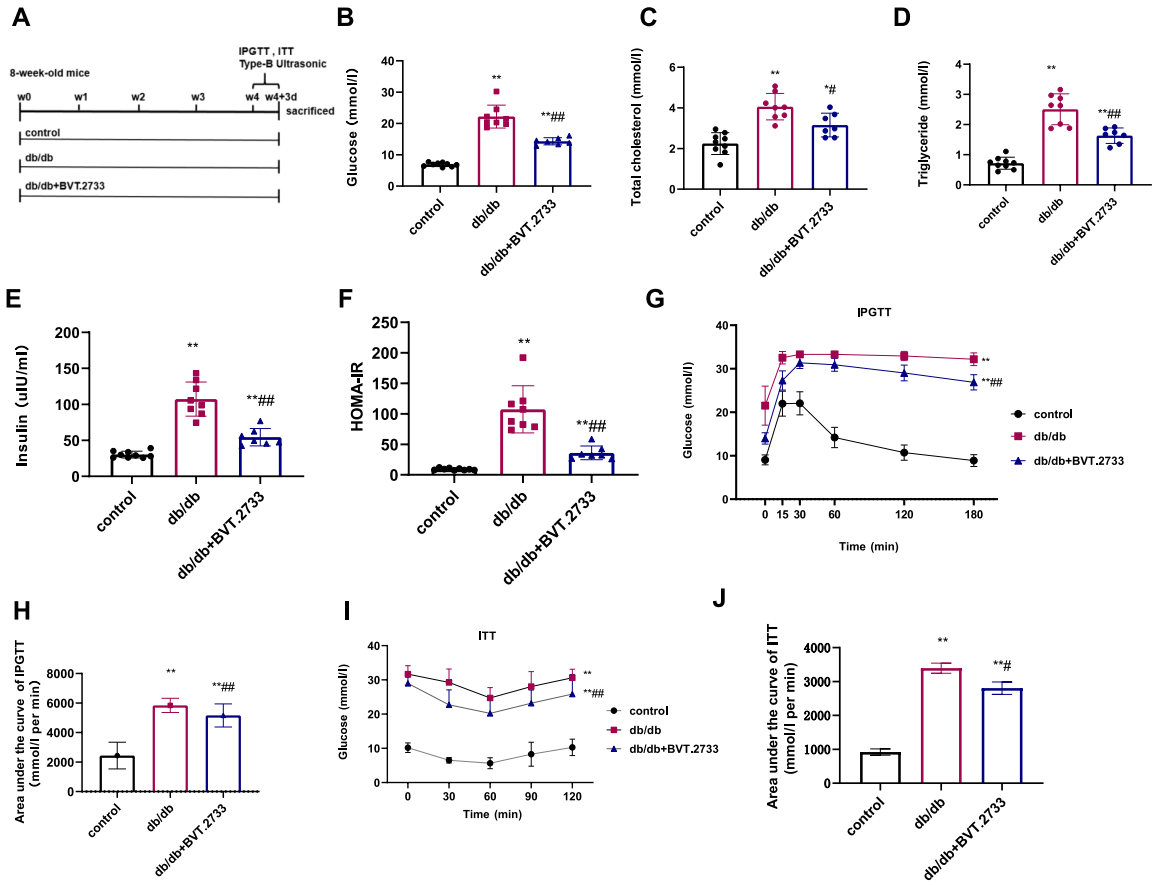

Fig. 1 BVT.2733 alleviates insulin resistance and glucolipid metabolism disorder in db/db mice. (A) Timeline of the experiment; (B) Glucose; (C) Total cholesterol; (D) Triglyceride; (E) Insulin; (F) HOMA-IR; (G) IPGTT; (H) Area under the curve of IPGTT; (I) ITT; (J) Area under the curve of ITT. ** $p < 0.01$, vs. control group. $^{\#}$ $p < 0.05$, $^{\#\#}$ $p < 0.01$, vs. db/db group.

whole liver, up-down diameter of the right liver lobe, anterior-posterior diameter of the right liver lobe, and anterior-posterior diameter of the left liver lobe ($p < 0.01$). Following BVT.2733 intervention, the up-down diameter of the right liver lobe decreased ($p < 0.05$) and the anterior-posterior diameter of the left liver lobe decreased ($p < 0.01$) (Fig. 2C). While there was no statistical difference in the other two diameters, the mean length of all four diameters was reduced, suggesting that BVT.2733 could relieve hepatomegaly (Fig. 2C).

Furthermore, BVT.2733 improved the degree of NAFLD, with moderate to severe NAFLD decreasing from 62% in the db/db group to 0% in the db/db +BVT.2733 group (Fig. 2D). Representative images of Type-B ultrasonic (Fig. 2E) showed increased echogenicity of the liver, blurring of intrahepatic vessels, and mild attenuation of the posterior beam in the db/db group compared with the control group, which were less pronounced in the db/db +BVT.2733 group.

HE staining (Fig. 2F) revealed that hepatocytes in the control group had clear hepatic lobules with normal morphology and structure. In contrast, hepatocytes in the db/db group showed diffuse fatty degeneration and obvious ballooning degeneration, which were alleviated by BVT.2733. The NAFLD activity score, used for a semi-quantitative assessment of NAFLD progression, increased in the db/db group compared with the control group ($p < 0.01$). However, after treatment with BVT.2733, the NAFLD activity score decreased ($p < 0.01$) (Fig. 2G).

Consistently, ORO staining (Fig. 2H) and the ORO staining-positive area (Fig. 2I) demonstrated that BVT.2733 alleviated lipid deposition. Collectively, these results indicate that BVT.2733 could alleviate NAFLD in db/db mice.

BVT.2733 decreases liver 11β-HSD1 and CORT levels

To investigate the inhibitory effect of BVT.2733 on liver 11β-HSD1 and CORT levels, we examined the expression of 11β-HSD1 and the levels of CORT in the

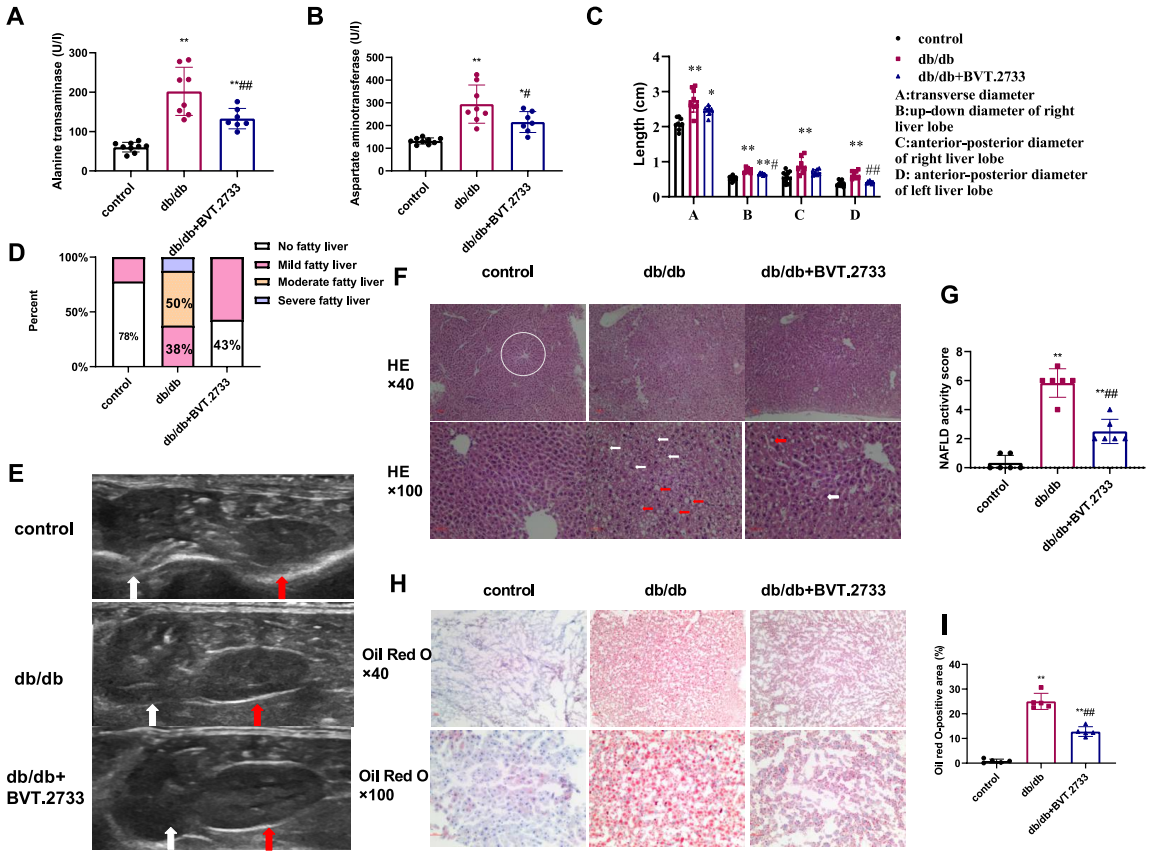

Fig. 2 BVT.2733 alleviates NAFLD in db/db mice. (A) Alanine transaminase; (B) Aspartate aminotransferase; (C) Comparisons of main diameters of mice liver by Type-B ultrasonic; (D) Proportion of NAFLD with different degrees; (E) Representative images of Type-B ultrasonic. The white arrow represents the mouse liver and the red arrow represents the mouse right kidney. (F) HE staining diagrams of mice liver (40x or 100x magnification). Scale bars 50 μm. The circle represents the structure of normal hepatic lobule. The white arrow represents the ballooning degeneration and the red arrow represents fatty degeneration. (G) NAFLD activity score; (H) ORO staining diagrams of mice liver, (40x or 100x magnification). Scale bars 50 μm. (I) ORO-positive area (%). ** $p < 0.01$, vs. control group. $^{\#}$ $p < 0.05$, $^{\#\#}$ $p < 0.01$, vs. db/db group.

liver. The expression of liver 11β-HSD1 in the db/db group was higher compared with the control group. Treatment with BVT.2733 led to a significant decrease in the expression of 11β-HSD1 ($p < 0.05$) (Fig. 3A).

Consistent with the decrease in 11β-HSD1 expression, BVT.2733 also reduced liver CORT levels ($p < 0.05$) (Fig. 3B). These findings indicate that BVT.2733 effectively decreases liver 11β-HSD1 expression and CORT levels in db/db mice.

BVT.2733 activates the PI3K/AKT signaling pathway and inhibits the mTOR signaling pathway

To investigate the molecular mechanism underlying the improvement of insulin resistance and NAFLD by BVT.2733, we assessed the expressions of proteins related to the PI3K-AKT-mTOR signaling pathway. Representative protein bands are shown in Fig. 4A. Results indicate that BVT.2733 increased the expression of p-PI3K ($p < 0.01$) (Fig. 4C) and p-AKT ($p < 0.05$) (Fig. 4E), while inhibiting the expression of p-mTOR ($p < 0.01$) (Fig. 4G). There were no statistically significant differences in the expressions of PI3K, AKT, and mTOR ($p > 0.05$) (Fig. 4B,D,F).

BVT.2733 promotes hepatocyte autophagy

To elucidate the effect of BVT.2733 on autophagy, we examined the expressions of autophagy-related proteins. Representative protein bands are shown in Fig. 5A. Compared with the db/db group, the expression of LC3II/I was increased ($p < 0.01$) (Fig. 5B), while the expression of P62 was decreased ($p < 0.05$) (Fig. 5C) in the liver tissue of the db/db +BVT.2733 group. These results suggest that BVT.2733 promotes hepatocyte autophagy.

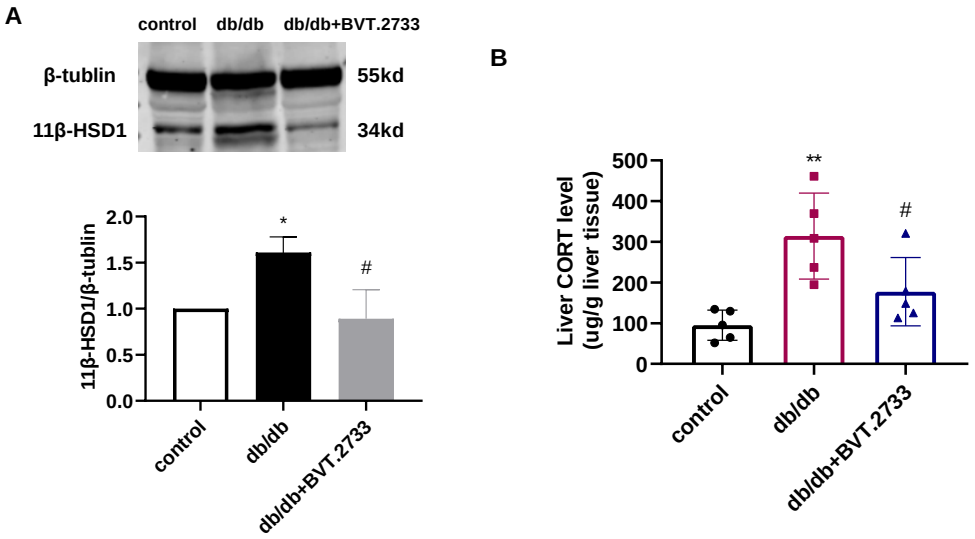

Fig. 3 BVT.2733 decreases liver 11β-HSD1 and CORT levels. (A) The representative protein bands and relative expression levels of 11β-HSD1 in liver tissues by Western blot. (B) Liver CORT levels by enzyme linked immunosorbent assay. * $p < 0.05$, ** $p < 0.01$ vs. control group. $^{\#}$ $p < 0.05$, vs. db/db group.

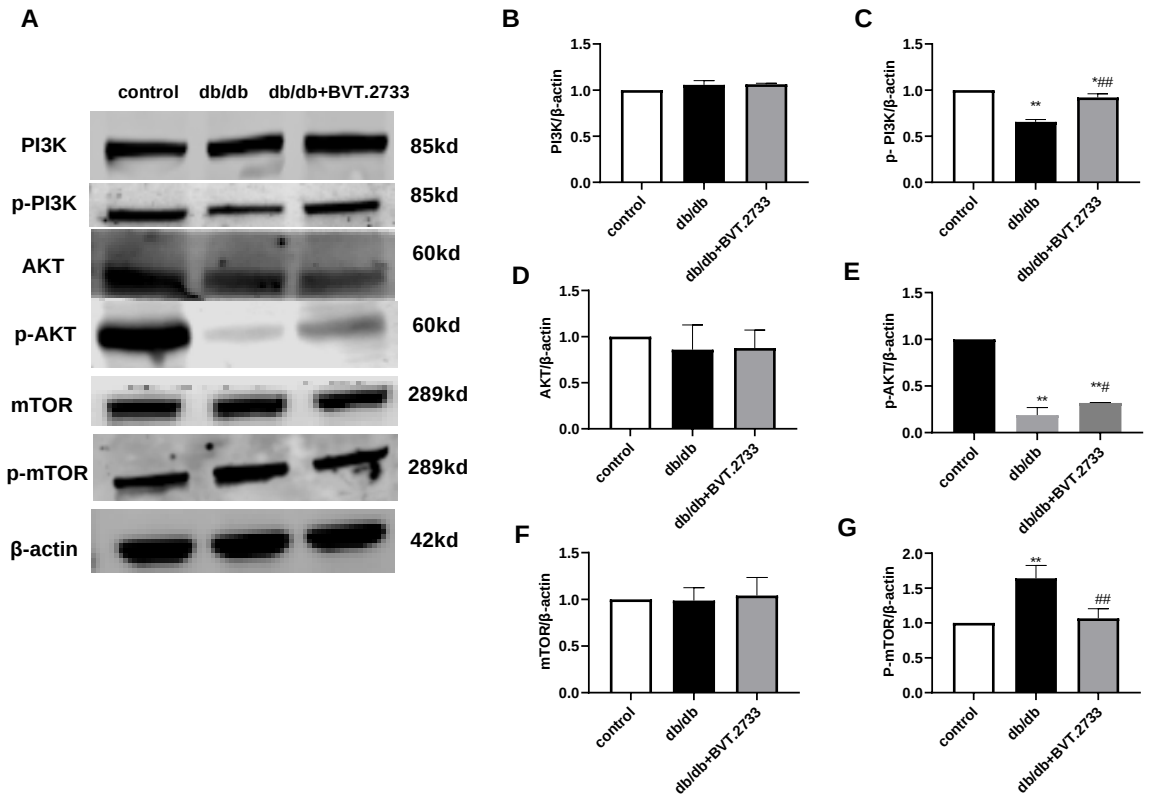

Fig. 4 BVT.2733 activates the PI3K/AKT signaling pathway and inhibits the mTOR signaling pathway. (A) The representative protein bands by Western blot. Relative expression levels of (B) PI3K, (C) p-PI3K, (D) AKT, (E) p-AKT, (F) mTOR and (G) p-mTOR in liver tissues by Western blot. * $p < 0.05$, ** $p < 0.01$ vs. control group. $^{\#}$ $p < 0.05$, $^{\#\#}$ $p < 0.01$, vs. db/db group.

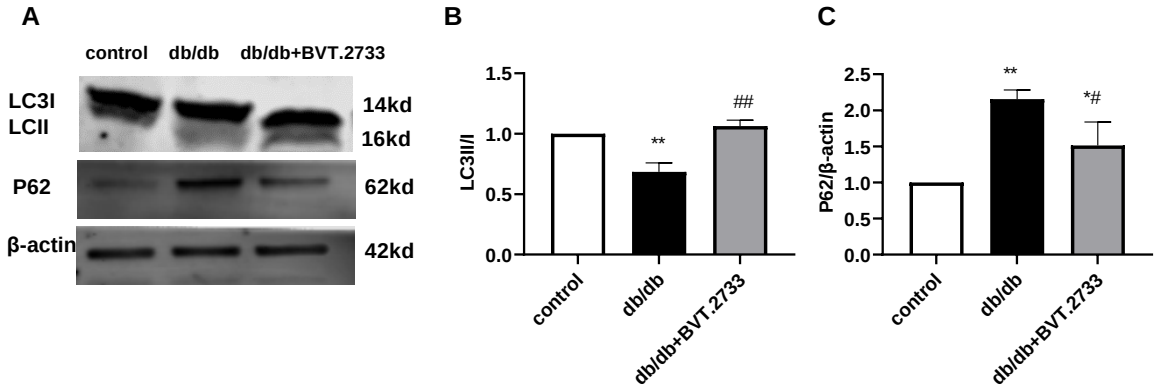

Fig. 5 BVT.2733 promotes hepatocyte autophagy. (A) The representative protein bands by Western blot. (B) Relative expression levels of LC3II/I and P62. * $p < 0.05$, ** $p < 0.01$ vs. control group. $^{\#}$ $p < 0.05$, vs. db/db group.

DISCUSSION

In this study, we observed that BVT.2733 improved glucose metabolism, lipid metabolism, and insulin resistance, consistent with previous literature [17]. The liver, an important target organ of insulin, is often associated with NAFLD in insulin resistance. NAFLD is characterized by hepatocyte steatosis without a history of excessive drinking. The spectrum of NAFLD includes simple fatty liver, steatohepatitis, fatty liver fibrosis, and cirrhosis, which vary with the disease's progression [18]. Our findings confirmed NAFLD in the db/db group using Type-B Ultrasonic. The db/db group exhibited increased serum alanine transaminase and aspartate aminotransferase levels, massive fatty degeneration, and ballooning degeneration, indicating that some mice in the db/db group progressed to steatohepatitis. BVT.2733 alleviated NAFLD from morphological to pathological aspects.

Liver 11β-HSD1 activity or expression is decreased during steatosis, serving as a protective mechanism to limit hepatic cortisol exposure and lipid accumulation. However, with the onset of steatohepatitis, 11β-HSD1 activity or expression increases [19]. Our study demonstrated that liver 11β-HSD1 expression in the db/db group was higher than that in the control group. BVT.2733 decreased liver 11β-HSD1 expression, thereby blocking glucocorticoid amplification. We hypothesized that elevated liver 11β-HSD1 expression leads to increased local CORT in the liver, contributing to NAFLD. Conversely, the administration of BVT.2733 reversed these effects.

Abnormalities in the insulin signaling pathway are crucial in the development of insulin resistance. The PI3K-AKT pathway is a classic insulin signaling pathway that, when activated, reduces liver gluconeogenesis by inhibiting the expressions of phosphoenolpyruvate carboxykinase and glucose-6-phosphatase. It also reduces the expression of glycogen synthase kinase-3β, promoting glycogen synthesis [20]. AKT promotes lipid synthesis and inhibits lipolysis through the mTOR1-RPS6KB1 pathway [8]. Numerous studies have shown that activating PI3K/AKT is beneficial in improving insulin resistance or related target organ damage [21–25]. Glucocorticoids directly inhibit the PI3K/AKT signaling pathway [21], potentially explaining how elevated liver CORT leads to insulin resistance and NAFLD. Our research demonstrated that the PI3K-AKT signaling pathway was inhibited in liver tissues of the db/db group but could be activated by BVT.2733.

mTOR is a downstream target of the PI3K-AKT signaling pathway and regulates various cellular processes, including gene transcription, protein translation, apoptosis, autophagy, cell cycle, and energy balance [26, 27]. In the early stages of diabetes, mTOR positively regulates the growth and insulin secretion of pancreatic β-cells. However, prolonged overactivation of mTOR leads to ineffective insulin secretion mechanisms and β-cell death [28]. In the liver, mTOR activation promotes hepatic insulin resistance by degrading IRS1, contributing to dysregulated glucose and lipid homeostasis [29]. Our research showed that p-mTOR expression increased in the db/db group compared with the control group, and this increase could be partially inhibited by BVT.2733. While PI3K-AKT is generally believed to positively regulate the mTOR signaling pathway [12]. Our research observed inconsistencies between the trends of PI3K-AKT and mTOR expression. This discrepancy could be explained by several factors. First, mTOR can downregulate the PI3K-AKT signaling pathway through feedback inhibition [30, 31]. Second, mTOR is affected not only by PI3K-AKT but also by adenosine monophosphate activated protein kinase (AMPK). Under insulin resistance, the AMPK signaling pathway is downregulated, leading to mTOR activation [11, 32]. The inhibitory effect of mTOR by PI3K-AKT is counterbalanced by AMPK activation, which activates mTOR [11, 12].

mTOR also plays a crucial role in regulating autophagy initiation, as its activation inhibits autophagy [10]. During autophagy, LC3I is enzymatically degraded to form LC3II [33]. P62 binds to ubiquitinated proteins and forms a complex with LC3-II, which is degraded in the autophagosome [34]. LC3II/I and P62 are hallmark proteins of autophagy [11]. To counteract the lipotoxic effects of free fatty acids, autophagy is induced and activated to maintain mitochondrial stability in hepatocytes, thus mitigating the lipotropic impact of free fatty acids. However sustained nutritional imbalance and abnormal insulin signaling pathways disrupt hepatic autophagy flow, leading to the onset of NAFLD [35]. Knocking down autophagy-related gene 5 results in increased hepatic triglycerides and lipid droplets [36], whereas the overexpression of autophagy-related gene 7 reduces endoplasmic reticulum stress and hepatic steatosis in obese mice, highlighting the importance of autophagy as a regulator [14]. Our research indicates that autophagy level of db/db group was lower than that in the control group, and BVT.2733 promoted autophagy. Autophagy has a certain protective effect on hepatic steatosis caused by insulin resistance. In addition, appropriate enhancement of autophagy can combat inflammation by inhibiting the transcription and maturation of pro-inflammatory cytokines, thereby aiding in mitigating the impact of inflammation on the liver and improving liver steatosis [37].

CONCLUSION

In summary, BVT.2733 improved glucose metabolism, lipid metabolism, and insulin resistance, and alleviated NAFLD in db/db mice. The mechanism may involve the decreased liver CORT levels and the promotion of hepatocyte autophagy, mediated by the PI3K-AKT and mTOR signaling pathways.

Acknowledgements: This work was supported by Open Research Funding of Central laboratory of Beijing Shijitan Hospital (2020-KF26). The funders had no role in study design, data collection and analysis, decision to publish, or preparation of the manuscript.

REFERENCES

1. Lee SH, Park SY, Choi CS (2022) Insulin resistance: From mechanisms to therapeutic strategies. *Diabetes Metab J* **46**, 15–37.
2. Carr RM, Correnti J (2015) Insulin resistance in clinical and experimental alcoholic liver disease. *Ann NY Acad Sci* **2015**, 1–20.
3. Piumngam K, Siriprungpong P, Roytrakul S (2021) Serum carbonic anhydrase combined with adiponectin as biomarkers of insulin resistance. *ScienceAsia* **47**, 287–292.
4. Gregory S, Hill D, Grey B, Ketelbey W, Miller T, Muniz-Terrera G, Ritchie CW (2020) 11β-hydroxysteroid dehydrogenase type 1 inhibitor use in human disease-a systematic review and narrative synthesis. *Metabolism* **108**, 154246.
5. Verma M, Sooy K, Just G, Nixon M, Morgan R, Andrew R, Chapman KE, Homer NZ (2020) Quantitative analysis of 11-dehydrocorticosterone and corticosterone for preclinical studies by liquid chromatography/triple quadrupole mass spectrometry. *Rapid Commun Mass Spec* **34**, e8610.
6. Yuan XH, Li HZ, Bai H, Zhao XJ, Zhang CL, Liu HF, Zhang YF, Zhao BH, et al (2016) The 11β-hydroxysteroid dehydrogenase type 1 inhibitor protects against the insulin resistance and hepatic steatosis in db/db mice. *Eur J Pharmacol* **788**, 140–151.
7. Abdallah BM, Beck-Nielsen H, Gaster M (2005) Increased expression of 11β-hydroxysteroid dehydrogenase type 1 in type 2 diabetic myotubes. *Eur J Clin Invest* **35**, 627–634.
8. Huang XJ, Liu GH, Guo J, Su ZQ (2018) The PI3K/AKT pathway in obesity and type 2 diabetes. *Int J Biol Sci* **14**, 1483–1496.
9. Li X, Wang J, Yang Q, Shao S (2017) 11β-Hydroxysteroid dehydrogenase type 1 in obese subjects with type 2 diabetes mellitus. *Am J Med Sci* **354**, 408–414.
10. Wang B, Zhong Y, Li Q, Cui L, Huang G (2018) Autophagy of macrophages is regulated by PI3k/Akt/mTOR signaling in the development of diabetic encephalopathy. *Aging* **10**, 2772–2782.
11. Álvarez-Mercado AI, Rojano-Alfonso C, Micó-Carnero M, Caballeria-Casals A, Peralta C, Casillas-Ramírez A (2021) New insights into the role of autophagy in liver surgery in the setting of metabolic syndrome and related diseases. *Front Cell Dev Biol* **9**, 670273.
12. Frendo-Cumbo S, Tokarz VL, Bilan PJ, Brumell JH, Klip A (2021) Communication between autophagy and insulin action: at the crux of insulin action-insulin resistance? *Front Cell Dev Biol* **9**, 1918.
13. Lin CW, Zhang H, Li M, Xiong X, Chen X, Chen X, Dong XC, Yin XM (2013) Pharmacological promotion of autophagy alleviates steatosis and injury in alcoholic and non-alcoholic fatty liver conditions in mice. *J Hepatol* **58**, 993–999.
14. Yang L, Li P, Fu SN, Calay ES, Hotamisligil GS (2010) Defective hepatic autophagy in obesity promotes ER stress and causes insulin resistance. *Cell Metab* **11**, 467–478.
15. Milton-Laskibar I, Aguirre L, Etxeberria U, Milagro FI, Martínez JA, Portillo MP (2018) Involvement of autophagy in the beneficial effects of resveratrol in hepatic steatosis treatment. A comparison with energy restriction. *Food Funct* **9**, 4207–4215.
16. Liu F, Yang H, Zhou WJ, Zhou XH (2014) Comparison of the characteristics of induced and spontaneous db/db mouse models of type 2 diabetes mellitus. *Acta Lab Anim Sci Sin* **74**, 54–59.
17. Wang L, Liu J, Zhang A, Cheng P, Zhang X, Lv S, Wu L, Yu J, et al (2012) BVT.2733, a selective 11β-hydroxysteroid dehydrogenase type 1 inhibitor, attenuates obesity and inflammation in diet-induced obese mice. *PLoS One* **7**, e40056.
18. Tanase DM, Gosav EM, Costea CF, Ciocoiu M, Lacatusu CM, Maranduca MA, Ouatu A, Floria M (2020) The intricate relationship between type 2 diabetes mellitus (T2DM), insulin resistance (IR), and nonalcoholic fatty liver disease (NAFLD). *J Diab Res* **2020**, 3920196.

19. Ahmed A, Rabbitt E, Brady T, Brown C, Guest P, Bujalska IJ, Doig C, Newsome PN (2012) A switch in hepatic cortisol metabolism across the spectrum of non-alcoholic fatty liver disease. *PLoS One* **7**, e29531.
20. Beaupere C, Liboz A, F'eve B, Blondeau B, Guillemain G (2021) Molecular mechanisms of glucocorticoid-induced insulin resistance. *Int J Mol Sci* **22**, 623.
21. Joharapurkar A, Dhanesha N, Shah G, Kharul R, Jain M (2012) 11β-Hydroxysteroid dehydrogenase type 1: Potential therapeutic target for metabolic syndrome. *Pharmacol Rep* **64**, 1055–1065.
22. Meng Y, Wang WW, Kang JS, Wang XX, Sun LK (2017) Role of the PI3K/AKT signalling pathway in apoptotic cell death in the cerebral cortex of streptozotocin-induced diabetic rats. *Exp Ther Med* **13**, 2417–2422.
23. Ostrovskaya RU, Yagubova SS, Gudasheva TA, Seredenin SB (2018) Antidiabetic Properties of low-molecular-weight BDNF mimetics depend on the type of activation of post-receptor signaling pathways. *Bull Exp Biol Med* **164**, 734–737.
24. Yang SS, Chen Z, Cao M, Li RJ, Wang ZG, Zhang MX (2017) Pioglitazone ameliorates Aβ42 deposition in rats with diet-induced insulin resistance associated with AKT/GSK3β activation. *Mol Med Rep* **15**, 2588–2594.
25. Song XF, Shao ZQ, Xu P (2022) Dexmedetomidine promotes cell proliferation and attenuates insulin resistance in high glucose induced trophoblast cells via inactivating the p38 MAPK pathway. *ScienceAsia* **48**, 734–739.
26. Talos DM, Sun H, Zhou X, Fitzgerald EC, Jackson MC, Klein PM, Lan VJ, Joseph A, et al (2012) The interaction between early life epilepsy and autistic-like behavioral consequences: A role for the mammalian target of rapamycin (mTOR) pathway. *PLoS One* **7**, e35885.
27. Bosco D, Fava A, Plastino M, Montalcini T, Pujia A (2011) Possible implications of insulin resistance and glucose metabolism in Alzheimer's disease pathogenesis. *J Cell Mol Med* **15**, 1807–1821.
28. Riahi Y, Wikstrom JD, Bachar-Wikstrom E, Polin N, Zucker H, Lee MS, Quan WY, Haataja L, et al (2016) Autophagy is a major regulator of beta cell insulin homeostasis. *Diabetologia* **59**, 1480–1491.
29. Burillo J, Marqués P, Jiménez B, González-Blanco C, Benito M, Guillén C (2021) Insulin resistance and diabetes mellitus in Alzheimer's disease. *Cells* **10**, 1236.
30. Khalid M, Alkaabi J, Khan MA, Adem A (2021) Insulin signal transduction perturbations in insulin resistance. *Int J Mol Sci* **22**, 8590.
31. Liu GY, Sabatini DM (2020) mTOR at the nexus of nutrition, growth, ageing and disease. *Nat Rev Mol Cell Biol* **21**, 183–203.
32. Schakman O, Kalista S, Barbé C, Loumaye A, Thissen JP (2013) Glucocorticoid-induced skeletal muscle atrophy. *Int J Biochem Cell Biol* **45**, 2163–2172.
33. Demirtas L, Guclu A, Erdur FM, Akbas EM, Ozcicek A, Onk D, Turkmen K (2016) Apoptosis, autophagy & endoplasmic reticulum stress in diabetes mellitus. *Indian J Med Res* **144**, 515–524.
34. Tanaka Y, Kume S, Kitada M, Kanasaki K, Uzu T, Maegawa H, Koya D (2012) Autophagy as a therapeutic target in diabetic nephropathy. *Exp Diab Res* **2012**, 628978.
35. Klionsky DJ, Petroni G, Amaravadi RK, Baehrecke EH, Ballabio A, Boya P, Pedro JMBS, Cadwell K, et al (2021) Autophagy in major human diseases. *EMBO J* **40**, e108863.
36. Singh R, Kaushik S, Wang Y, Xiang Y, Novak I, Komatsu M, Tanaka K, Cuervo AM, et al (2009) Autophagy regulates lipid metabolism. *Nature*, **458**, 1131–1135.
37. Wu W, Zhang L, Chan M (2018) Autophagy, NAFLD and NAFLD-Related HCC. *Adv Exp Med Biol* **1061**, 127–138.